Thin Solid Films 518 (2010) 2825–2829

Contents lists available at ScienceDirect

Thin Solid Films

journal homepage: www.elsevier.com/locate/tsf

Element-specific electronic structure of Mn dopants and ferromagnetism of (Zn,Mn)O thin films

J. Jin [a], G.S. Chang [b], D.W. Boukhvalov [c,d], X.Y. Zhang [a,*], L.D. Finkelstein [c], W. Xu [a], Y.X. Zhou [a], E.Z. Kurmaev [c], A. Moewes [b]

[a] Department of Physics, Surface Physics Laboratory (National Key Laboratory) and Synchrotron Radiation Research Center of Fudan University, 220 Handan Road, Shanghai 200433, China
[b] Department of Physics and Engineering Physics, University of Saskatchewan, 116 Science Place, Saskatoon, SK, Canada S7N 5E2
[c] Institute of Metal Physics, Russian Academy of Sciences-Ural Division, Yekaterinburg 620219, Russia
[d] Institute for Molecules and Materials, Radboud University, 6525 ED Nijmegen, The Netherlands

ARTICLE INFO

Article history:
Received 27 February 2009
Received in revised form 5 November 2009
Accepted 19 December 2009
Available online 4 January 2010

Keywords:
Soft X-ray spectroscopy
Electronic structure
Ferromagnetism
(Zn,Mn)O

ABSTRACT

Element-specific electronic structure of (Zn,Mn)O thin films with various Mn concentrations has been investigated using X-ray absorption and emission spectroscopy. According to comparison between the experimental spectra and the density functional theory calculations (partial density of states and exchange interactions for various Mn defect configurations), the substitutional Mn impurities do not induce ferromagnetism in (Zn,Mn)O samples. The ferromagnetic properties can be obtained when defect configurations consisting of both substitutional and interstitial Mn atoms are present. The ferromagnetism in ZnO-based magnetic semiconductors is favored to be Ruderman–Kittel–Kasuya–Yoshida type and the established theoretical model is in a good agreement with the X-ray spectroscopic measurements.

1. Introduction

Transition metal-doped semiconductors, called diluted magnetic semiconductors (DMSs) have attracted great attention in recent years since they are being considered as key components for spintronic applications [1–3]. Among promising candidates, Mn-doped ZnO has been studied extensively, which was motivated by the theoretical prediction of ferromagnetism in this system at room temperature (RT) [4]. Ferromagnetic (FM) behaviors of (Zn,Mn)O systems have been experimentally observed both at low temperature (~45 K) and RT [5–10], although ferromagnetism has not been established in polycrystalline samples prepared under thermal equilibrium conditions [11]. Meanwhile, the controversy has swelled around the issue whether ferromagnetism in the ZnO-based DMS materials is carrier-induced (*intrinsic*) or due to the formation of Mn-related secondary phases (*extrinsic*). Several mechanisms such as the Ruderman–Kittel–Kasuya–Yoshida (RKKY) interaction [12], the double exchange interaction [13], and the Zener model [4] have been proposed to shed light on the origin of ferromagnetism. However, the situation became even more complicated when paramagnetic or antiferromagnetic (AFM) behaviors were also observed in (Zn,Mn)O materials [14,15]. That is why it is highly desirable to understand the origin of various forms of magnetism in (Zn,Mn)O. Since the magnetic properties of (Zn,Mn)O systems are known to strongly correlate with an exchange interaction between magnetic impurity atoms, an approach to study the local electronic structure near them in detail is promising.

In the present study, we performed *ab initio* calculations of electronic structure and exchange interactions in (Zn,Mn)O system based on different defect configurations and compared our results to soft X-ray absorption/emission spectroscopy measurements. Our results suggest that the ferromagnetism results from interstitial Mn atoms interacting with the adjacent substitutional Mn atoms. A RKKY-type exchange interaction is directly observed in our samples.

2. Experimental details

The $Zn_{1-x}Mn_xO$ thin films with various Mn concentrations ($x = 0.03$, 0.06, 0.11, 0.20, and 0.33) were grown by a molecular beam epitaxy on Si (100) substrate with a ZnO buffer layer. The substrate temperature and oxygen partial pressure were kept constant at 200 °C and 1.06×10^{-3} Pa, respectively. According to vibrating sample magnetometry measurements, the $Zn_{1-x}Mn_xO$ samples with low Mn concentration ($x = 0.03$, 0.06, and 0.11) exhibit FM behaviors while the AFM coupling is observed for the samples with 20 and 33% of Mn concentration. The Curie temperature (T_C) of $Zn_{1-x}Mn_xO$ with $x = 0.03$ is about 45 K. The AFM behaviors of the heavy-doped samples are attributed to a formation of MnO secondary phase as confirmed by X-ray diffraction (XRD) and extended X-ray absorption fine structure (EXAFS)

* Corresponding author. Tel.: +86 21 65643522; fax: +86 21 65643626.
E-mail address: xy-zhang@fudan.edu.cn (X.Y. Zhang).

0040-6090/$ – see front matter © 2009 Elsevier B.V. All rights reserved.
doi:10.1016/j.tsf.2009.12.100

analysis. It was found that for the Mn concentration above 20%, MnO clusters begin to be formed and become dominant in the sample with the highest Mn concentration of 33%. Details of the crystalline structure and magnetic properties are present in Ref. [16].

Element-specific X-ray absorption and emission spectroscopy (XAS and XES, respectively) measurements were carried out at Beamline 8.0.1 of the Advanced Light Source at Lawrence Berkeley National Laboratory. The Mn 2*p* and O 1*s* XAS spectra (in total electron yield mode) as well as resonant Mn $L_{2,3}$ ($3d4s \rightarrow 2p$ transition) and nonresonant O *K*α ($2p \rightarrow 1s$ transition) XES spectra were recorded at RT. All measured spectra were normalized to the number of photons falling on the sample monitored by a highly transparent gold mesh.

3. Results and discussion

Fig. 1(a) and (b) shows the Mn 2*p* XAS (top) and Mn $L_{2,3}$ resonant X-ray emission spectra (RXES) of $Zn_{1-x}Mn_xO$ thin films ($x = 0.06$ and 0.33). Although the absorption lines of $Zn_{0.94}Mn_{0.06}O$ sample is very weak due to low Mn concentration, the multiplet structure of both samples with $x = 0.06$ and 0.33 are similar to that of divalent Mn ions (Mn^{2+}) [17]. An additional feature present at 639 eV in Mn 2*p* XAS for $Zn_{0.67}Mn_{0.33}O$ thin film is typical for MnO with relatively a large crystal-field interaction [17,18]. To obtain the detailed electronic structure of occupied Mn 3*d* states, Mn $L_{2,3}$ RXES spectra were obtained at various excitation energies (E_{exc}), three at L_3 and two at L_2 edges. It is clear that the overall spectral features strongly depend on the E_{exc} and are different between the lightly and heavily doped samples. For the RXES spectra, two peaks at about 3−5 eV below the elastic peak (labelled *1* and *2* in Fig. 1) are attributed to *d*−*d* excitations, which correspond to transitions to different L_3 multiplet states. These *d*–*d* excitation features are sensitive to the local interaction between Mn atoms and their nearest neighbours because the XES process occurs in the first coordination sphere of the emitting atom. Fig. 1(c) represents the change in two *d*–*d* excitation features with respect to Mn concentration. One can see that Mn L_2 emission lines shift toward lower emission lines while increasing Mn content in ZnO. A similar trend can be found in Mn $L_{2,3}$ nonresonant X-ray emission spectra (NXES) taken at the E_{exc} well above the L_2 absorption threshold as shown in Fig. 1(d). The small shoulder at 637 eV of $Zn_{0.97}Mn_{0.03}O$ grows significantly and becomes dominant for the $Zn_{0.67}Mn_{0.33}O$ sample. This reflects that the hybridization between Mn 3*d* and O 2*p* orbitals in a heavily doped sample is much stronger than that in the same with low Mn concentration.

On the other hand, we investigated O 1s XAS and O *K*α XES spectra of $Zn_{1-x}Mn_xO$ thin films and the results are present in Fig. 2. The O *K*α NXES spectra exhibits three subbands labelled *a*, *b* and *c*. The features are contributed from O 2*p* states hybridized with Zn 3*d*, 4*s*, and 4*p* states. Subbands *b* and *c* become less pronounced with increasing Mn concentration and vanish for $x = 0.33$ while the feature *a* shifts toward lower emission energy and becomes broader with increased Mn doping. In the O 1*s* XAS spectra displayed in Fig. 2(b), the main feature B shifts toward higher absorption energies with increasing Mn concentration. For the samples with high Mn concentrations ($x = 0.20$ and 0.33), an additional feature labelled A′ appears. According to our electronic structure calculations (see below), these spectral changes arise from the formation of different defects consisting of substitutional and/or interstitial Mn impurity atoms.

When a DMS film is grown under non-equilibrium conditions, the impurity atoms can occupy not only cation sites but also interstitial

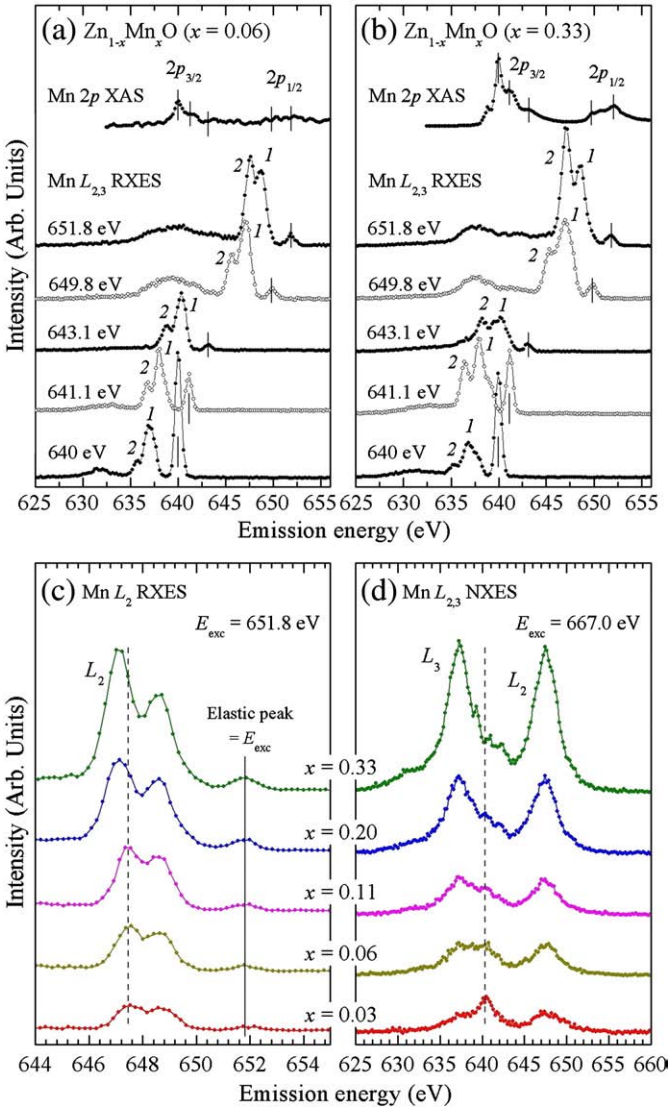

Fig. 1. Mn 2*p* XAS spectra (top) and Mn $L_{2,3}$ RXES spectra of $Zn_{1-x}Mn_xO$ thin films with $x = 0.06$ (a) and 0.33 (b), and Mn L_2 RXES spectra ($E_{exc} = 651.8$ eV) (c) and Mn $L_{2,3}$ NXES spectra ($E_{exc} = 667$ eV) (d) of $Zn_{1-x}Mn_xO$ ($x = 0.03$, 0.06, 0.11, 0.20, and 0.33). The vertical bars in RXES spectra in the top panels indicate the corresponding excitation energies shown in the XAS spectra.

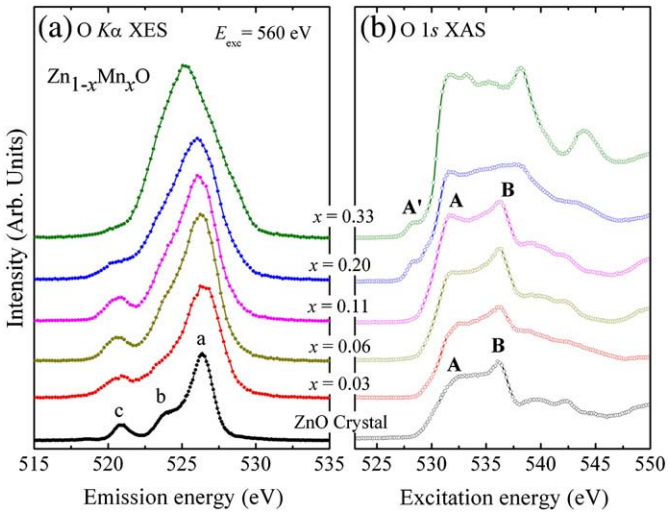

Fig. 2. O *K*α NXES spectra ($E_{exc} = 560$ eV) (a) and O 1*s* XAS spectra (b) of $Zn_{1-x}Mn_xO$ thin films ($x = 0.03$, 0.06, 0.11, 0.20, and 0.33). The emission and absorption spectra of ZnO single-crystal reference sample are added for comparison (bottom).

sites [19,20]. Therefore, the presence of interstitial sites should be taken into account when calculating the electronic structure and magnetic properties. The concentrations of these defects depend on the energy required for their formation written as [21]:

$$E_{\text{form}}(q) = E_{\text{T}}(q) - n_{\text{Zn}}\mu_{\text{Zn}} - n_{\text{O}}\mu_{\text{O}} - n_{\text{Mn}}\mu_{\text{Mn}} + qE_{\text{F}}, \quad (1)$$

where, $E_{\text{T}}(q)$ is the total energy of the supercell with a defect in charge state q, n_{Zn} (n_{Mn} and n_{O}) stands for the number of Zn atoms (Mn and O) in the supercell, μ_{Zn} (μ_{Mn} and μ_{O}) is the atomic chemical potential and E_{F} is the Fermi energy. We have used a Zn-rich limit where $\mu_{\text{O}} = \mu_{\text{ZnO}} - \mu_{\text{Zn}}$ and μ_{Zn} are the calculated chemical potentials for the bulk Zn-structure (*P*63/*mmc*).

It is important to note that our samples were grown at 200 °C, which is considerably lower than typical growth temperatures (600–800 °C) of $Zn_{1-x}Mn_xO$ samples [19]. This means that the various defect configurations are not equally probable in our samples and the samples reported by others [10,20]. In order to identify which defects are most likely present in our systems, we have calculated their formation energies using the SIESTA program [22]. We performed geometry optimizations for a $4a \times 4a \times 4c$ supercell containing of 32 Zn and 32 O atoms. Three kinds of defect configurations were considered: (1) single substitutional and interstitial defects (labelled *S* and *I*, respectively), (2) paired defects for the combination of single defects in one unit cell (*S*–*S*, *S*–*I*, and *I*–*I*, etc) and (3) pairs of single defects in different cells, which are not directly connected (or via one oxygen) (2*S*, *SI*, and 2*I*, etc). The following formation energy values for neutral systems ($q = 0$) with different defect configurations were obtained: $S = -3.16$ eV, S–$S = -2.87$ eV, $I = 0.74$ eV, S–$I = 0.93$ eV, $3S$–$I = 1.32$ eV, $6S$–$I = 1.64$ eV. The calculation suggests that Mn-related defects requiring minimal formation energy are most likely and this is found to be for the defect scenarios *S*, *I*, *SI*, *S*–*I*, and *S*–*S*. It is reasonable to consider that the single defects are dominant in the lightly doped samples. Although the formation energy for *S*–*S* defect is lower than that of single interstitial defect *I*, the *S*–*S* and *S*–*I* contents may be negligible due to low Mn concentration.

For better understanding of element-specific XAS and XES results, the electronic structure of (Zn,Mn)O lattices was calculated. Different Mn concentrations were simulated by varying the Mn–Mn distance. That is, high Mn concentration corresponds to a short interatomic distance between nearest Mn impurities in the ZnO lattice. We used the following five configurations of *S*–*S*, *2S*, *S*–*I*, *SI* and 2*I* defects corresponding to different Mn–Mn distances, and calculated the electronic structure and exchange interactions of (Zn,Mn)O using the linearized muffin-tin-orbital method in the atomic-spheres approximation (LMTO-ASA) (Stuttgart TB-47) [23]. It is found that the substitutional-only defects (*S*–*S* and 2*S*) exhibit the antiferromagnetic exchange interaction (exchange value, $J = 255$ meV) with minimal distances between Mn atoms and the strength of exchange interaction is exponentially reduced for longer Mn–Mn distances. This means that the ferromagnetism cannot be induced if all Mn atoms substitute for cation sites. It is in accordance with other experimental [20,24] and theoretical [19,24–26] results. Therefore, we can rule out the influence of substitutional-only defects on the FM behavior of our $Zn_{1-x}Mn_xO$ samples with low Mn concentrations.

Fig. 3 shows the calculated partial density of states (pDOS) of Mn 3*d* and O 2*p* orbitals in the double-defect configurations for different Mn concentrations (*SI* for $x = 0.03$, *S*–*I* for $x = 0.20$, and *S*–*S* for $x = 0.33$ $Zn_{1-x}Mn_xO$). One can see that the spectral weight of the main Mn 3*d* states (feature *1*) shifts toward lower (negative) energies (i.e. retraction of *d*-density from the Fermi level) and the low-energy subband (feature 2) is relatively insensitive to change with Mn concentration when the *S*–*S* pairs are present. However, as seen in Fig. 1(c) and (d), the energy position of this feature from experimental spectra does not change with increase of the Mn concentration. This supports that the *S*–*S* pairs are not induced or at least negligible in the entire set of samples. On the other hand, Fig. 3(b) shows that the low-energy Mn 3*d* subband (feature *2*) is caused by the hybridization of Mn 3*d* with O 2*p* orbitals. It is prominent that the features a and b are influenced by the presence of Mn defects.

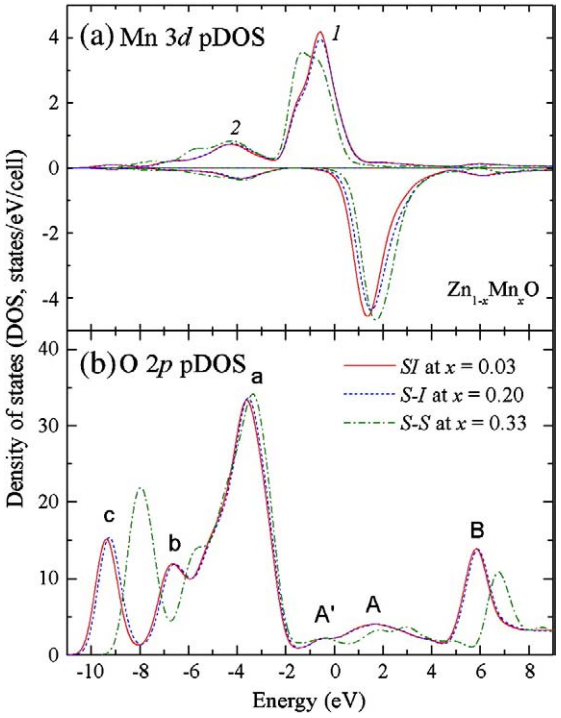

Fig. 3. Calculated pDOS of spin-resolved Mn 3*d* (a) and O 2*p* states (b) for $Zn_{1-x}Mn_xO$ lattices with $x = 0.03$, 0.20, and 0.33.

After calculating the pDOSs of Mn and O atoms in (Zn,Mn)O structure, we compared them with experimental Mn L_3 and O $K\alpha$ NXES spectra, as shown in Fig. 4. The fine structure of experimental spectra is fairly reproduced by the calculated pDOSs. Especially, for the $Zn_{1-x}Mn_xO$ sample with $x = 0.03$, the spectral features are fairly similar with those calculated for (Zn,Mn)O structure with *SI* defects. The relative intensity between features *1* and *2* is completely changed by doping large amount of Mn. The experimental Mn L_3 NXES spectrum of 33% Mn-doped ZnO samples exhibits a dominant feature *2* and this cannot be reproduced by the electronic structure calculation even for the (Zn,Mn)O structure with the same Mn concentration containing the *S*–*S* pairs. Once again, this result indicates the absence of *S*–*S* pairs in our samples. The prominence of Mn 3*d*-O 2*p* hybridized states (feature 2) for 33% Mn-doped ZnO sample can be attributed to the formation of the MnO secondary phases while the calculation is based on a wurtzite ZnO lattice. This is in accordance with XRD and EXAFS characterization [16].

Although a comparison of experimental XES spectra and calculated electronic structure of (Zn,Mn)O thin films reveals that FM samples with low Mn concentrations contain the Mn interstitial-related defect without any indication of the presence of *S*–*S* defects, the influence of these defect configurations on magnetic properties of our samples still needs to be addressed. That is why we calculated the exchange interactions for *SI* and 2*I* configurations by a method described in Ref. [27]. The calculational results are displayed in Fig. 5. The exchange interaction between Mn atoms was found to oscillate as a function of distance between them, as expected in the RKKY model. A weak FM interaction can be observed for both defect configurations with Mn–Mn distances from 3.8 to 4.2 Å for Mn concentration of 20%. In case of *SI* configuration, it is observed for a Mn–Mn distances from 4.2 to 5.3 Å, which corresponds to the Mn concentrations of 3–11%. With increased Mn concentration to 33% (i.e. a decrease in Mn–Mn

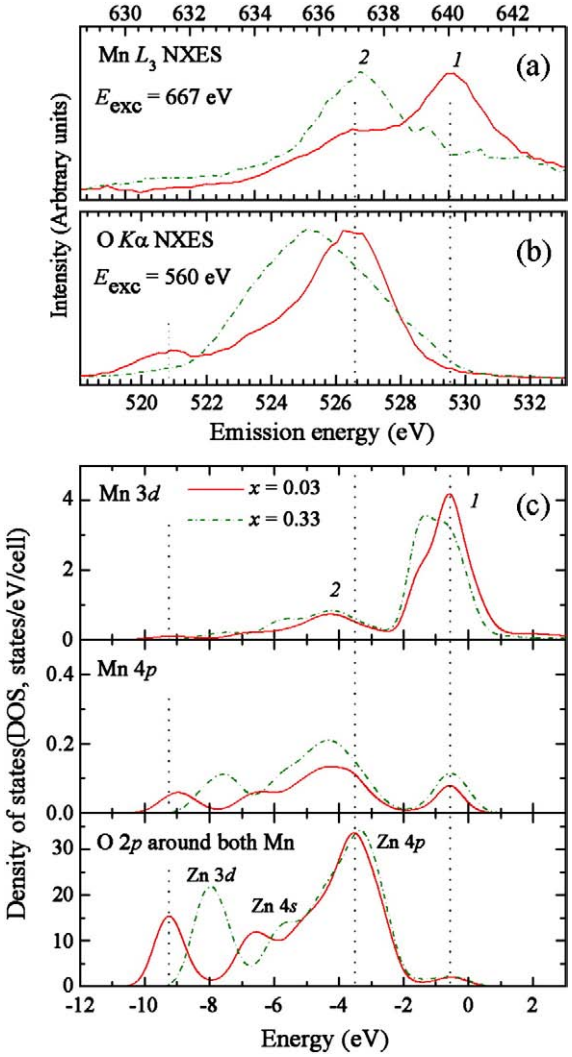

Fig. 4. Comparison of experimental Mn L_3-region NXES spectra (a) and O $K\alpha$ NXES spectra (b) of $Zn_{1-x}Mn_xO$ thin films ($x = 0.03$ and 0.33) with calculated pDOS of Mn 3*d*, Mn 4*p*, and O 2*p* orbitals (c) of $Zn_{1-x}Mn_xO$ systems for $x = 0.03$ and 0.33. Each calculated pDOS for $x = 0.03$ and 0.33 corresponds to *SI* and *S–S* configurations, respectively.

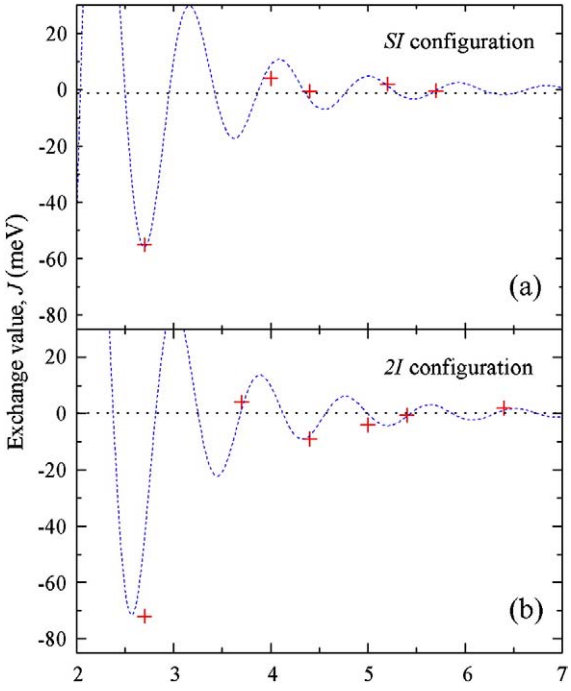

Fig. 5. Exchange interactions between Mn atoms versus their distance in (Zn,Mn)O. Red crosses — calculated values; blue dashed lines — RKKY model fitting, for *SI* (a) and *2I* (b) configurations.

distance), the formation of AFM coupling pairs can take place between the nearest neighbours. From the exchange interaction values, we can calculate T_C using the following equation:

$$T_C = NJS(S+1)/3k_B \quad (2)$$

where N is the total number of exchange pairs and S is the spin of magnetic atoms. In case of low Mn concentrations, a two-dimensional network is formed and therefore N will be equal to 4. Discontinuities are likely present in real non-ideal materials. When substituting $N = 4$ with $N = 3$, T_C can reach a value of 48 K (in the *SI* configuration), which is astonishingly close to the experimental value of 45 K [16]. Therefore, a weak FM exchange interaction in (Zn,Mn)O materials can be realized at the expense of *SI* interactions and the RKKY model provides a very important method for understanding ferromagnetism in DMSs. This is a direct observation of RKKY interaction in the ZnO-based DMS system.

4. Conclusions

To conclude, we have investigated the electronic structure of constituent elements (Mn and O) of $Zn_{1-x}Mn_xO$ using soft X-ray absorption and emission spectroscopy. The experimental spectra were compared to *ab initio* calculations in order to shed light on the origin of ferromagnetism in ZnO-based DMS systems. The overall results reveal that Mn interstitial defects are present in FM samples with low Mn concentrations, as concluded from the behavior of calculated Mn 3*d* main-band and the experimental Mn L_3 XES spectra. The ferromagnetism in $Zn_{1-x}Mn_xO$ thin films with lower Mn concentrations originates from the exchange interaction in the interstitial-related defect configuration. For samples with high Mn concentrations, it was found that most of Mn dopants form a MnO secondary phases and exhibit antiferromagnetic behavior. Our study strongly suggests that ferromagnetism in (Zn,Mn)O DMS system is mostly of the RKKY-type.

Acknowledgements

This work was supported by special fund for Major State Basic Research of China Project No. G2001CB3095, the Project of the State Key Program of National Natural Science Foundation of China (Grant No. 10635060), the Discovery Grant from Natural Sciences and Engineering Research Council of Canada (NSERC), RAS Program (Project 01.2.006 13395), the Research Council of the President of the Russian Federation (Grant NSH-3572.2010.2, the Russian Science Foundation for Basic Research (Project 08-02-00148). DWB acknowledges support from Stichting voor Fundamenteel Onderzoek der Materie (FOM), The Netherlands.

References

[1] H. Ohno, Science 281 (1998) 951.
[2] S.A. Wolf, D.D. Awschalom, R.A. Buhrman, J.M. Daughton, S. von Molnar, M.L. Roukes, A.Y. Chtchelkanova, D.M. Treger, Science 294 (2001) 1488.
[3] Ü. Özgür, Ya.I. Alivov, C. Liu, A. Teke, M.A. Reshchikov, S. Doğan, V. Avrutin, S.-J. Cho, H. Morkoç, J. Appl. Phys. 98 (2005) 041301.
[4] T. Dietl, H. Ohno, F. Matsukura, J. Cibert, D. Ferrand, Science 287 (2000) 1019.
[5] U. Philipose, Selvakumar V. Nair, S. Trudel, C.F. de Souza, S. Aouba, R.H. Hill, H.E. Ruda, Appl. Phys. Lett. 88 (2006) 2631101.

[6] L.B. Duan, G.H. Rao, J. Yu, Y.C. Wang, W.G. Chu, L.N. Zhang, J. Appl. Phys. 102 (2007) 103907.
[7] S. Banerjee, K. Rajendran, N. Gayathri, M. Sardar, S. Senthilkumar, V. Sengodan, J. Appl. Phys. 104 (2008) 043913.
[8] M. Schumm, M. Koerdel, S. Müller, H. Zutz, C. Ronning, J. Stehr, D.M. Hofmann, J. Geurts, New J. Phys. 10 (2008) 043004.
[9] A. Di Trolio, C. Veroli, A.M. Testa, D. Fiorani, Superlattices Microst. 46 (2009) 101.
[10] T. Meron, G. Markovich, J. Phys. Chem. B 109 (2005) 20232.
[11] J. Alaria, P. Turek, M. Bernard, M. Bouloudenine, A. Berbadj, N. Brihi, G. Schmerber, S. Colis, A. Dinia, Chem. Phys. Lett. 415 (2005) 337.
[12] F. Matsukura, H. Ohno, A. Shen, Y. Sugawara, Phys. Rev. B 57 (1998) R2037.
[13] H. Akai, Phys. Rev. Lett. 81 (1998) 3002.
[14] H.J. von Baradeleben, J.L. Cantin, E. Chikoidze, A. Mauger, J. Appl. Phys. 101 (2007) 013902.
[15] K. Masuko, A. Ashida, T. Yoshimura, N. Fujimura, J. Appl. Phys. 103 (2008) 043714.
[16] W. Xu, Y.X. Zhou, X.Y. Zhang, D.L. Chen, Y.N. Xie, T. Liu, W.S. Yan, S.Q. Wei, Solid State Commun. 141 (2007) 374.
[17] J.-S. Kang, S.W. Han, J.-G. Park, S.C. Wi, S.S. Lee, G. Kim, H.J. Song, H.J. Shin, W. Jo, B.I. Min, Phys. Rev. B 71 (2005) 092405.
[18] S.M. Butorin, J.-H. Guo, M. Magnusson, P. Kuiper, J. Nordgren, Phys. Rev. B 54 (1996) 4405.
[19] G.S. Chang, E.Z. Kurmaev, D.W. Boukhvalov, L.D. Finkelstein, S. Colis, T. Pedersen, A. Moewes, A. Dinia, J. Phys. Condens. Matter 19 (2007) 276210.
[20] M. Bouloudenin, N. Vart, S. Colis, J. Kortus, A. Dinia, Appl. Phys. Lett. 87 (2005) 052501.
[21] F. Oba, S.R. Nishitani, S. Isotani, H. Adachi, J. Appl. Phys. 90 (2001) 824.
[22] J.M. Soler, E. Artacho, G.D. Gale, A. Garsia, J. Junquera, P. Ordejon, D. Sanchez-Portal, J. Phys. Condens. Matter 14 (2002) 2745.
[23] O.K. Andersen, Phys. Rev. B 12 (1975) 3060.
[24] J. Alaria, M. Bouloudenin, G. Schmerber, S. Colis, A. Dinia, J. Appl. Phys. 99 (2006) 08M118.
[25] G.S. Chang, E.Z. Kurmaev, D.W. Boukhvalov, L.D. Finkelstein, D.H. Kim, T.-W. Noh, A. Moewes, T.A. Callcott, J. Phys. Condens. Matter 18 (2006) 4243.
[26] Q. Wang, Q. Sang, B.K. Rao, P. Jena, Phys. Rev. B 69 (2004) 233310.
[27] Y.-J. Zhao, T. Shishidou, A.J. Freeman, Phys. Rev. Lett. 90 (2003) 047204.